Polarization-transparent microphotonic devices in the strong confinement limit

TYMON BARWICZ*§, MICHAEL R. WATTS†, MILOŠ A. POPOVIĆ, PETER T. RAKICH, LUCIANO SOCCI‡, FRANZ X. KÄRTNER, ERICH P. IPPEN AND HENRY I. SMITH

Research Laboratory of Electronics, Massachusetts Institute of Technology, 77 Massachusetts Ave, Cambridge, Massachusetts 02139, USA
***Present address: IBM T.J. Watson Research Center, Yorktown Heights, New York, USA**
†Present address: Sandia National Laboratory, Albuquerque, New Mexico, USA
‡Permanent address: Pirelli Labs S.p.A, Milan, Italy
§e-mail: tymon@alum.mit.edu

Published online: 21 December 2006; doi:10.1038/nphoton.2006.41

Microphotonic structures that strongly confine light, such as photonic crystals and micron-sized resonators, have unique characteristics that could radically advance technology[1–6]. However, such devices cannot be used in most applications because of their inherent polarization sensitivity; they respond differently to light polarized along different axes[7–9]. To take advantage of the distinctive properties of these structures, a general, integrated, broadband solution to their polarization sensitivity is needed. Here, we show the first demonstration of such a solution. It enables arbitrary, polarization-sensitive, strong-confinement (SC) microphotonic devices to be rendered insensitive (transparent) to the input polarization at all wavelengths of operation. To test our approach, we create the first polarization-transparent add–drop filter from polarization-sensitive microring resonators. It shows almost complete elimination of polarization sensitivity over the 60-nm bandwidth measured, while maintaining outstanding filter performance. This development is a milestone for SC microphotonics, allowing the applications of photonic-crystal and microring devices to several areas, including communications, spectroscopy and remote sensing.

Polarization sensitivity is a major problem in microphotonics, because the polarization state changes randomly in optical fibres. This makes SC microphotonic devices incompatible with the optical fibres necessary to connect them to the outside world. SC microphotonics should not be confused with microphotonics using weak confinement of light, such as those based on doped-silica waveguides and ridge waveguides, as these may be fabricated to be individually polarization transparent[10–12]. This is impossible for SC microphotonic devices as it would require fabrication with subatomic absolute dimensional accuracy (see Supplementary Information). Ridge waveguides, even those made in silicon, are not considered part of SC microphotonics as they offer a weak lateral field confinement that results in substantial bending loss and, consequently, in large resonator size. However, a ridge waveguide etched so deep that it resembles a rectangular waveguide and shares a similar level of confinement will also exhibit similar challenges in polarization transparency.

Our approach to polarization transparency is based on polarization diversity with a unique implementation that exploits symmetry to overcome sensitivities to fabrication imperfections that would otherwise prohibit practical applications. Polarization-transparent devices are constructed from polarization-sensitive components using the integrated scheme shown in Fig. 1. The arbitrary polarization state emanating from a fibre is split into orthogonally polarized components travelling in separate arms. By rotating the polarization state in one of these arms, a single polarization is realized on-chip. The two arms then pass through identical sets of polarization-sensitive photonic structures. At the output of the chip, another polarization rotation is performed and the two arms are recombined. The second polarization rotation is carried out to avoid wave interference between the two arms, and the

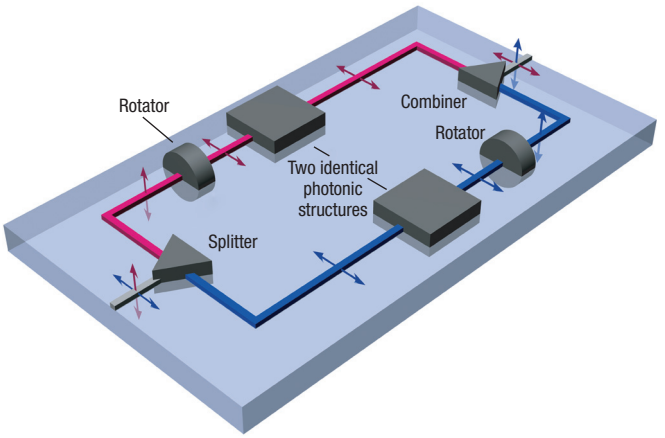

Figure 1 Integrated polarization diversity scheme. Polarization-transparent microphotonic circuits are constructed from polarization-sensitive components. Arrows depict the orientation of the electric field. An arbitrary input polarization state is split into its orthogonal components and one of these components is rotated to achieve a single on-chip polarization state. Two identical copies of arbitrarily polarization-sensitive photonic structures are used for the two arms of the architecture. At the output, the two arms are recombined after one of the polarization components is rotated to prevent interference between the two signals.

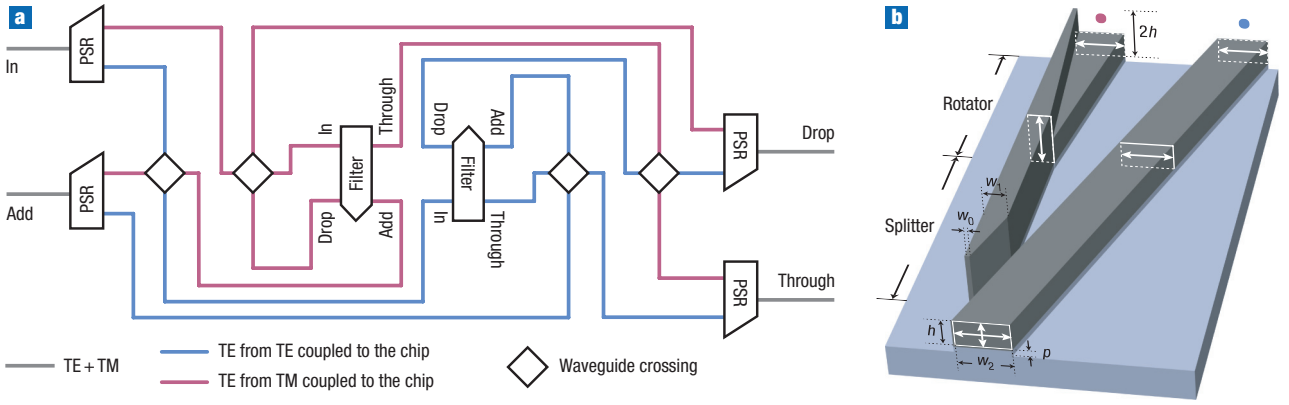

Figure 2 Design of the polarization-transparent optical add–drop filter (OADF). a, Functional diagram of the OADF. **b**, Schematic of the polarization splitter and rotator (PSR). The white arrows depict the orientation of the electric field in the guides. The vertically polarized light (TM mode) tunnels across the small gap to the tall waveguide and the horizontally polarized light (TE mode) remains in the flat waveguide. The values of the parameters are $w_0 = 70$ nm, $w_1 = 360$ nm, $w_2 = 800$ nm, $p = 100$ nm and $h = 420$ nm. The PSR is about 600 μm long. The waveguide on the right remains straight and its cross-section unchanged along the length of the PSR. The left waveguide is separated from the right waveguide by 200 nm at the onset of the splitter. This separation grows to 1 μm before the onset of the rotator. The width of the top layer of the rotator is slowly reduced from w_1 to w_0, and the width of the bottom layer is increased from w_1 to w_2. This twisting waveguide induces polarization rotation by mimicking the chirality naturally produced by large molecules found in nature.

rotators are placed on opposite arms to achieve overall symmetry. In Fig. 1, the photonic structures depicted operate on the transverse-electric (TE) polarization state, corresponding to an in-plane orientation of the electric field. By rearranging the polarization rotators in the circuit, it is straightforward to construct a polarization diversity scheme for photonic structures operating on the transverse-magnetic (TM) polarization state.

We demonstrate integrated polarization diversity through the realization of a polarization-transparent optical add–drop filter (OADF) from polarization-sensitive microring resonators. For the resonances of a microring to be spaced sufficiently far apart for wavelength-division multiplexing (WDM) applications, the microring must be small, with a radius of a few microns. For the light to travel efficiently around such sharp bends, it must be tightly confined to the ring waveguide. Such confinement calls for a high refractive-index contrast between the waveguide core and its surroundings. In this work, silicon-rich silicon nitride (SiN) ($n = 2.193$ at 1,550 nm) waveguides are used. The waveguides sit on a silicon oxide ($n = 1.455$ at 1,550 nm) undercladding and are surrounded by air on the top and sides. As with all SC microphotonic devices, obtaining an identical response in such microrings for the two orthogonal polarization states is all but impossible in practice, because it would require picometre-level absolute dimensional control at fabrication.

A schematic of the polarization-transparent add–drop filter is presented in Fig. 2a. Light of unknown polarization is coupled to the chip from a fibre. First, it reaches a polarization splitter and rotator (PSR), where the light is split into its TE and TM polarization eigenstates, and the TM component is subsequently rotated to become TE. The two components are then directed towards two identical OADFs. Finally, the light passes through another PSR before exiting the chip towards a fibre. This second PSR is traversed in the reverse direction so that the thus-far nonrotated TE polarized light is rotated to become TM and combined with the other light component. This system is twofold symmetric and the inputs may be used as outputs. To our knowledge, the successful realization of an SC microphotonic circuit of this complexity has not yet been reported. However, it is of the minimum complexity required to render completely arbitrary photonic structures polarization transparent.

The PSRs used are shown in Fig. 2b. They were designed so that it is energetically favourable for the vertically polarized light (TM mode) to tunnel across the narrow gap into the tall waveguide, but the horizontally polarized light (TE mode) remains in the flat waveguide. The TM polarization state is then rotated to become TE by slowly transforming the tall waveguide into a flat one through a structure that emulates a twisting waveguide and mimics the chirality naturally exhibited by large molecules found in nature. The transformations in the PSR are remarkably effective and adiabatic: no coupling between the various modes of the structure is desired. These PSRs have negligible intrinsic loss and allow a >300-nm bandwidth of polarization-transparent operation. The design of the PSR is reported in refs 13 and 14 and its earliest experimental demonstration in ref. 15.

A micrograph of the middle part of the fabricated structure is presented in Fig. 3a. The PSRs are not shown and extend to the left and the right of the micrograph. Each OADF is formed from three stages of third-order serially coupled microring filters. The light entering an OADF at the resonant wavelength is extracted from the input waveguide and transferred to the output (drop) waveguides by means of the resonant microring chain. The multistage configuration improves the extinction of the dropped wavelength in the through port[16]. This is critical, because any remaining signal will act as noise to an added data stream. The waveguide crossings are formed from waveguides that widen adiabatically from 600-nm-wide at the edges of the crossings to 3-μm-wide near the centre to suppress undesirable crosstalk and loss. The design of the filters and crossings is described in the Methods section.

The polarization-transparent OADF is a two-layer structure. In fact, breaking the vertical symmetry is fundamentally necessary for rotating polarization. The PSR uses the top and bottom layers, and the filters and crossings use the bottom layer only. The structure was fabricated by an innovative fabrication technique illustrated in Fig. 3c–i. Instead of defining the two layers one at a

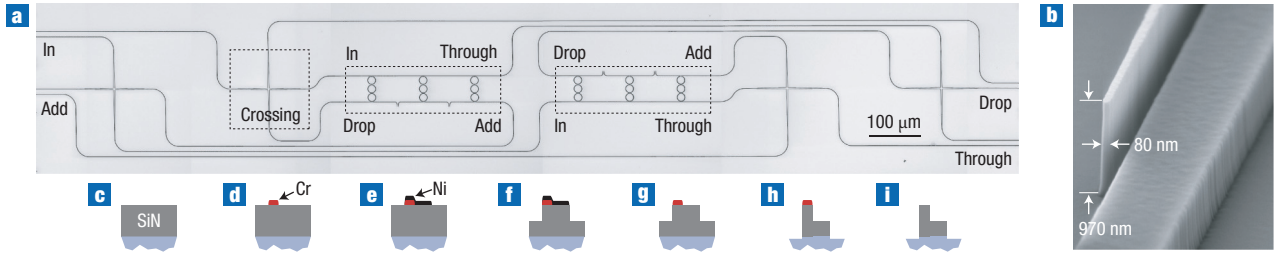

Figure 3 Fabricated polarization-transparent OADF. a, Electron micrograph of the central part of a fabricated polarization-transparent OADF. The PSRs are not shown and extend to the left and the right of the micrograph. The picture was assembled from six successive micrographs and the greyscale was inverted to make the fine lines readable when printed. **b**, Electron micrograph of the onset of a polarization splitter. The finest features show an aspect ratio of more than 12:1. **c–i**, Illustration of the novel fabrication technique used to create the bilevel structures. The technique is described in detail in the Methods section.

time, the SiN required for the both is deposited at the same time. The patterns corresponding to the two layers are registered in two distinct hard masks on top of the SiN, and successive etches and hard-mask removals are applied. This fabrication process is described in more detail in the Methods section.

The optical performance of the fabricated polarization-transparent OADF is presented in Fig. 4 for 40 randomly chosen polarization states at every wavelength. In addition, independently acquired responses of the two polarization eigenstates are overlaid in colour. An extraordinarily low polarization-dependent loss (PDL) with a mean of 1.0 dB and a standard deviation across the spectrum of 0.45 dB is achieved. Of this PDL, 0.3 dB is due to the optical characterization scheme, which is described in the Methods section. The measured polarization-transparent bandwidth exceeds 60 nm. In Fig. 4, the PDL is the vertical distance between the blue and the red curves. Without the polarization diversity scheme, the underlying microrings would show a spectral misalignment of several nanometres between the responses of the two polarization eigenstates. Here, the spectral misalignment is negligible. Defining a misalignment figure of merit as the free spectral range of a resonator (20 nm in this work) divided by the spectral misalignment, we obtain, without any postfabrication trimming, 1,180 for the drop port and 540 for the through port. These remaining spectral misalignments correspond to slight differences in resonant frequency between the two, nominally identical, multistage microring filters in the OADF. The resonant frequencies are controlled at fabrication through the average ring-waveguide width of each microring. The through-port spectral misalignment corresponds to a remarkable relative control of the average ring-waveguide widths of all 18 microrings of the OADF to 0.15 nm, and the drop-port spectral misalignment corresponds to a relative control of the average ring-waveguide widths of the 6 microrings of the first stages of the two filters to 0.07 nm. This relative dimensional control was achieved through precise adjustments of the electron beam (e-beam) exposure dose of the various microrings and a tailored e-beam writing strategy[17]. Relative control is to be distinguished from absolute dimensional control, which is impossible to achieve to such an extent.

The fabricated polarization-transparent OADF shows a remarkable through-port extinction of more than 32 dB and a drop loss of no more than 2 dB. Its bandwidth spans 50 GHz (0.40 nm), its free spectral range reaches 2.5 THz (20 nm), and it allows a minimum channel spacing of 130 GHz (1.05 nm). The transmission between the add and the through port is not shown, but is almost identical to the transmission between the input and the drop port. The polarization sensitivity on the bottom of the through-port response is of no consequence as it is below the 30-dB extinction required in OADFs. The spectral oscillations, particularly visible off-resonance in the through-port response, are due to a shortcoming of the scanning electron-beam lithography system that was used. This is explained in greater detail in the Supplementary Information.

The demonstration of integrated polarization diversity opens a path for the construction of polarization-transparent SC microphotonic circuits from arbitrarily polarization-sensitive SC microphotonic components. The efficacy of this approach was tested rigorously by realizing the first polarization-transparent OADF from polarization-sensitive SC microring resonators. The resulting SC microphotonic circuit is, to our knowledge, the most complex achieved to date. It demonstrates almost complete elimination of polarization sensitivity over the

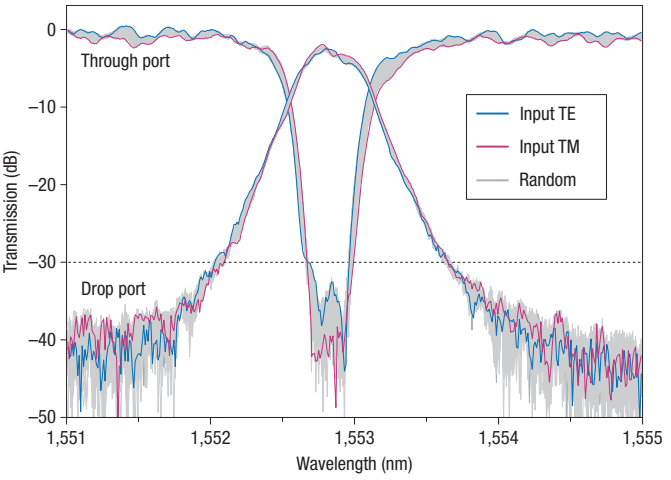

Figure 4 Spectral response of a fabricated polarization-transparent OADF for 40 randomly chosen polarization states at each wavelength. The spectral responses for the two polarization eigenstates are overlaid in blue and red. A remarkably low polarization-dependent loss (the vertical distance between the responses of the two eigenstates) with a mean of 1.0 dB and standard deviation of 0.45 dB is demonstrated. Of the shown polarization-dependent loss, 0.3 dB is due to the optical characterization setup. The polarization-transparent operation was designed to exceed a 300-nm bandwidth and was confirmed over the 60-nm bandwidth measured. This is achieved without any postfabrication trimming and while maintaining spectacular filter performance. The shape of the spectral response below the −30 dB line is of no consequence.

60-nm bandwidth measured, while maintaining outstanding device performance. Polarization transparency is a key milestone for SC microphotonics, allowing the immediate application of photonic-crystal devices and micrometre-scale resonators to numerous disciplines, including communications, spectroscopy and remote sensing.

METHODS

DESIGN

Each OADF was formed from three cascaded third-order microring filters. The third-order filters were designed with a flat-top (Chebyshev) drop-port response[18], broadened for minimum impact of loss. The SC microring resonators were designed by a vector-field leaky resonant mode solver, and the coupling gaps determined using three-dimensional finite-difference time-domain (3D FDTD) simulations. The filter design details are reported in refs 16 and 19. The waveguide crossings were designed with 3D FDTD. Each waveguide was expanded adiabatically until the field of the fundamental mode at the waveguide edges was negligible and the large lateral extent of the mode guaranteed slow diffraction. The design of the PSR was also performed with 3D FDTD and is reported in refs 13 and 14.

FABRICATION

The fabrication process is illustrated in Fig. 3c–i. First, Si wafers are thermally oxidized to form a 3-μm SiO_2 undercladding. Then 840 nm of SiN is deposited using low-pressure chemical-vapour deposition (Fig. 3c). Next, 200 nm of polymethylmethacrylate (PMMA) and 50 nm of Aquasave are spun on. Aquasave is a water-soluble conductive polymer from Mitsubishi Rayon (Tokyo, Japan) used to prevent charging during e-beam lithography. The pattern of the top layer is exposed using a Raith 150 (Raith GmbH, Dortmund, Germany) scanning electron-beam lithography (SEBL) system operating at 30 keV. The Aquasave is removed and the PMMA is developed. Then, 55 nm of Cr is e-beam evaporated and a lift-off performed by removing the non-exposed PMMA (Fig. 3d). A second hardmask is similarly defined using PMMA, Aquasave, SEBL and lift-off. This time, however, the hardmask is formed from 45-nm-thick Ni, the pattern corresponds to the bottom layer, and the Raith 150 SEBL exposure is aligned to the existent Cr pattern (Fig. 3e). Conventional reactive-ion etching (RIE) is used with a gas mixture of CHF_3 and O_2 to etch the SiN to a depth corresponding to the height of the bottom layer (Fig. 3f). The Ni hardmask is stripped (Fig. 3g) and a second RIE applied, defining the height of the top layer and transferring down the unprotected pattern of the bottom layer (Fig. 3h). The structure is etched 100 nm into the SiO_2. Finally, the Cr hardmask is stripped (Fig. 3i). The etch depths are controlled by alternating short RIE steps with profilometer measurements. The SEBL dose is carefully adjusted across the patterns to allow good dimensional control on a wide range of feature sizes (70–3,000 nm) and matching of the resonance frequencies of the 18 microrings forming the filter[17].

CHARACTERIZATION

Optical characterization entailed point-by-point laser transmission measurements. Specific polarization states were generated with a tunable laser and an electronic polarization controller and were coupled into and out of the waveguides with lensed fibres. The chip does not use high-efficiency fibre-to-chip couplers, but the waveguide cross-section at the chip facets was designed to offer polarization transparent coupling efficiency (low but equal efficiencies for both polarizations; see Supplementary Information). The collected laser line was then spectrally filtered with a synchronously tuned monochromator (to reject amplified spontaneous emission in the laser) and detected with an InGaAs PIN photodiode through lock-in detection. The TE and TM eigenstates were reliably identified through extinction of the TE and TM resonances of stand-alone ring resonators on the optical chip. The drop loss was measured by comparing the optical power in the through and drop ports at the output of the chip. To avoid biasing the measurement by fibre-to-chip coupling efficiency variations, the measurement was repeated several times on numerous devices. As the filter through-port loss off-resonance has been experimentally verified to be negligible, the drop loss represents the input-to-output waveguide net loss, near the filter. A polarization extinction of at least 16 dB was measured here on stand-alone PSRs in the 60-nm bandwidth of interest. As all signals travel via two PSRs, the resulting polarization crosstalk is at least 32 dB and correspondingly limits the through-port extinction of the add–drop filter.

Received 7 June 2006; revised 26 October 2006; accepted 5 November 2006; published 21 December 2006.

References

1. Vlasov, Y. A., O'Boyle, M., Hamann, H. F. & McNab, S. J. Active control of slow light on a chip with photonic crystal waveguides. *Nature* **438,** 65–69 (2005).
2. Soljačić, M. & Joannopoulos, J. D. Enhancement of nonlinear effects using photonic crystals. *Nature Mater.* **3,** 211–219 (2004).
3. Akahane, Y., Asano, T., Song, B.-S. & Noda, S. High-Q photonic nanocavity in a two-dimensional photonic crystal. *Nature* **425,** 944–947 (2003).
4. Song, B.-S., Noda, S. & Asano, T. Photonic devices based on in-plane hetero photonic crystals. *Science* **300,** 1537 (2003).
5. Hill, M. T. *et al.* A fast low-power optical memory based on coupled micro-ring lasers. *Nature* **432,** 206–209 (2004).
6. Almeida, V. R., Barrios, C. A., Panepucci, R. R. & Lipson, M. All-optical control of light on a silicon chip. *Nature* **431,** 1081–1084 (2004).
7. Pavesi, L. & Lockwood, D. J. Silicon Photonics (Springer, New York, 2004).
8. Manolatou, C., Johnson, S. G., Fan, S., Villeneuve, P. R., Haus, H. A. & Joannopoulos, J. D. High-density integrated optics. *J. Lightwave Technol.* **17,** 1682–1692 (1999).
9. Sadot, D. & Boimovich, E. Tunable optical filters for WDM applications. *IEEE Commun. Mag.* **36,** 50–55 (1998).
10. Headley, W. R., Reed, G. T., Howe, S., Liu, A. & Paniccia, M. Polarization-independent optical racetrack resonators using rib waveguides on silicon-on-insulator. *Appl. Phys. Lett.* **85,** 5523–5525 (2004).
11. Xu, D.-X., Janz, S. & Cheben, P. Design of polarization-insensitive ring resonators in silicon-on-insulator using MMI couplers and cladding stress engineering. *IEEE Phot. Technol. Lett.* **18,** 343–345 (2006).
12. Kwan, C. H. & Chiang, K. S. Study of polarization-dependent coupling in optical waveguide directional couplers by the effective-index method with built-in perturbation correction. *J. Lightwave Technol.* **20,** 1018–1026 (2002).
13. Watts, M. R., Haus, H. A. & Ippen, E. P. Integrated mode-evolution-based polarization splitter. *Opt. Lett.* **30,** 967–969 (2005).
14. Watts, M. R. & Haus, H. A. Integrated mode-evolution-based polarization rotators. *Opt. Lett.* **30,** 138–140 (2005).
15. Watts, M. R. *et al.* Towards integrated polarization diversity: design, fabrication, and characterization of integrated polarization splitters and rotators. *2005 Optical Fiber Communications Conference Postdeadline Papers* (IEEE Cat. No. 05CH37672), Part 5, Vol. **5** (2005).
16. Popovic, M. A. *et al.* Multistage high-order microring-resonator add-drop filters, *Opt. Lett.* **31,** 2571–2573 (2006).
17. Barwicz, T. *et al.* Fabrication of add-drop filters based on frequency-matched microring resonators. *J. Lightwave Technol.* **24,** 2207–2218 (2006).
18. Melloni, A. & Martinelli, M. Synthesis of direct-coupled-resonators bandpass filters for WDM systems. *J. Lightwave Technol.* **20,** 296–303 (2002).
19. Popovic, M. A. *et al.* High-index-contrast, wide-FSR microring-resonator filter design and realization with frequency-shift compensation, presented at the *Optical Fiber Communication Conference OFC/NFOEC'05*, Anaheim, CA, 2005, paper OFK1.

Acknowledgements

This project resulted from the vision of Hermann A. Haus. We thank Minghao Qi for contributing to the development of the fabrication process. This work was supported by Pirelli Labs S.p.A (Milan, Italy) through the leadership of M. Romagnoli and made use of MIT's SEBL facility in the Research Laboratory of Electronics (SEBL at RLE).
Supplementary information accompanies this paper on www.nature.com/naturephotonics.
Correspondence and requests for materials should be addressed to T.B. (tymon@alum.mit.edu).

Author contributions

T.B. and M.R.W. contributed equally to this work. T.B. developed the nanofabrication techniques required for this work and created the polarization-transparent OADF. M.R.W. proposed the integrated-polarization-diversity approach, designed the PSR and the waveguide crossings, and co-designed the microring filters.

Competing financial interests

The authors declare that they have no competing financial interests.